

High-resolution Fourier transform infrared and cw-diode laser cavity ringdown spectroscopy of the $\nu_2+2\nu_3$ band of methane near 7510 cm^{-1} in slit jet expansions and at room temperature

Michael Hippler and Martin Quack

Physical Chemistry, ETH Zürich, CH-8093 Zürich, Switzerland

(Received 4 September 2001; accepted 15 November 2001)

The $\nu_2+2\nu_3$ combination band of $^{12}\text{CH}_4$ near 7510 cm^{-1} was studied with the recently introduced technique of cavity ring-down spectroscopy employing a cw-diode laser in a pulsed supersonic slit jet expansion and with Doppler-limited Fourier-transform infrared spectroscopy at room temperature. $\nu_2+2\nu_3$ is the strongest absorption band in the high-wave-number region of the $N=2.5$ icosad of methane. First assignments of the combination band are provided. The vibrational origin of $\nu_2+2\nu_3$ at $7510.3378\pm 0.0010\text{ cm}^{-1}$, the integrated band strength $G=(1.3\pm 0.2)\times 10^{-4}\text{ pm}^2$ and the vibrational transition moment $|\mu_\nu|=(1.0\pm 0.1)\times 10^{-3}\text{ D}$ have been determined. The values represent benchmarks to test effective vibrational Hamiltonians and *ab initio* calculations for methane. Although an isolated band analysis was possible at low J -values, the influence of strong perturbations becomes evident at higher rotational excitation. The F_1 -component of $\nu_2+2\nu_3$ interacting by a strong Coriolis resonance with the IR-active F_2 -component appears to be a dominant perturber. © 2002 American Institute of Physics. [DOI: 10.1063/1.1433505]

I. INTRODUCTION

The analysis of overtone spectra allows the study of intramolecular dynamics of molecules in highly vibrationally excited states, for example, to extract mechanisms and time scales of intramolecular vibrational redistribution processes.¹⁻⁶ In many cases, however, homogeneous and inhomogeneous broadening and spectral congestion gives rise to unresolved, broad rotational contours preventing a line-by-line rovibrational assignment and analysis to extract the more detailed dynamic information. With low moments of inertia and thus large rotational constants, overtone spectra of methane are more easily rotationally resolved, particularly if supersonic jet cooling removes rotational hot-band congestion.^{7,8} The assignment and analysis of methane isotopomer spectra then allows testing effective Hamiltonians⁹⁻¹² and provides a database for analytical applications and for modeling of spectra, for example, under interstellar and planetary conditions. It is also feasible to perform accurate calculations in full dimensionality on *ab initio* and empirically refined potential hypersurfaces,¹³⁻²² which are to be compared with experiment.

Considering simple harmonic oscillator and rigid spherical top models, IR spectra of methane might at first be expected to be rather simple. However, rotation-vibration (Coriolis) interactions spoil the simplicity by lifting the degeneracy of rovibrational levels.^{23,24} In addition, strong Fermi resonances exist between CH-stretching and bending modes.^{9,24} Vibrational levels are thus grouped into resonance polyads, characterized by the common polyad quantum number $N=v_1+v_3+0.5\times(v_2+v_4)$, where v_1 and v_3 represent CH-stretching and v_2 and v_4 CH-bending quanta.²⁴ Each vibrational band is divided into different subbands classified by the T_d point group symmetry; they are in general strongly

mixed by Coriolis interactions. At sufficient spectral resolution, rovibrational transitions are found to split into components due to the nuclear spin isomers of $^{12}\text{CH}_4$, ortho-methane with total nuclear spin $I=1$ and relative abundance $x=9/16$ at room temperature, meta-methane with $I=2$ and $x=5/16$ and para-methane with $I=0$ and $x=2/16$. These isomers represent essentially three different modifications of methane, since approximate nuclear spin symmetry conservation^{25,26} prevents their conversion by optical transitions and collisions at least on short time scales,^{7,8} including in a more general way also chemical reactions.²⁵⁻²⁷ At longer time scales, though, nuclear spin isomers may interconvert.^{28,29} Overtone spectra of methane thus contain rich information, but they are rather complex and difficult to analyze. At present, the rovibrational analysis of overtone spectra for polyads up to $N=1.5$ is very advanced, and work is in progress to model also the $N=2$ polyad (tetradecad).^{8,24,30-33} The analysis of higher polyads, however, is still at its very beginnings. To record weak overtone spectra of methane under room-temperature and jet-cooling conditions, new experimental spectroscopic techniques are very helpful.

Cavity ring-down (CRD) spectroscopy with cw lasers is a new technique, which combines very high resolution, extreme sensitivity and the ability to measure absorbances directly.³⁴⁻³⁷ High sensitivity is an obvious requirement for analytical applications, but also important for certain fundamental investigations of intramolecular dynamics, where intrinsically very weak transitions are to be measured. Absorbances are required to quantify the concentration of absorbing species, if their absorption cross section is known, or to determine cross sections and integrated band strengths, which are needed as data base for spectroscopic analysis, to derive experimental dipole moment functions^{13,15} or to test

ab initio calculations or model Hamiltonians. High resolution increases the selectivity of spectroscopy and allows recovering most detailed molecular information, if rotational line-resolved spectra are obtained. This will in general require the use of cw lasers, since pulsed laser systems have a large bandwidth, at best Fourier-transform limited, thus limiting the effective resolving power of pulsed CRD spectroscopy.^{38,39} High-resolution spectroscopy is best combined with supersonic slit jet expansions to minimize Doppler broadening, to avoid pressure broadening and to remove rotational hot-band congestion by jet cooling, which will greatly simplify the assignment of rotationally resolved spectra.

Recently, we introduced a new approach to cw-CRD spectroscopy,^{36,37} which allows very sensitive high-resolution spectroscopy in pulsed slit jet expansions, and we characterized the technique by showing some nitrous oxide and methane overtone transitions.³⁷ In the present study, we apply the technique in combination with Doppler-limited FTIR measurements to obtain the high-resolution absorption spectrum of the $\nu_2 + 2\nu_3$ combination band of methane near 7510 cm^{-1} , and we present an analysis and first assignments of this band prevailing in the high-wave-number region of the $N=2.5$ icosad.

II. EXPERIMENT

In CRD spectroscopy with diode lasers, monochromatic light is coupled into an optical cavity composed of high-reflectivity mirrors, and then switched-off. Light intensity within the cavity will then decay due to losses on the mirrors and also due to absorbing gas-phase molecules by an exponential decay with decay constant k ,

$$k = \alpha c + (1 - R)c/l. \quad (1)$$

The decay is monitored outside the cavity. c is the speed of light. $R \approx 1$ is essentially the reflectivity of the mirrors, but also includes nonresonant losses by scattering and diffraction. Since R is essentially constant, the second term in Eq. (1) is the spectral baseline. The absorption coefficient α is related to the absorption cross section $\sigma = \alpha/C$, where C is the particle density of the absorbing species inside the cavity. Light is typically reflected back and forth several thousand times in the cavity during the time for the measured decay signals, resulting in effective absorption path lengths of several km. The absorbance per pass A_{pp} given by Eq. (2) is an appropriate quantity for jet measurements, where concentrations are not uniform and in general not known,

$$A_{pp} \equiv \ln(I_0/I) = \alpha l. \quad (2)$$

The experimental setup employed for CRD spectroscopy at room temperature and in pulsed supersonic slit jet expansions has been described in detail before.^{36,37} In short, after coupling light from a near-infrared cw diode into an optical cavity and then switching-off the laser via an acousto-optical modulator, the decaying light intensity is observed by a photodiode. Matching the cavity length to the laser wavelength is achieved by a simple passive scheme, where the cavity length is periodically varied using a piezoelectric transducer.

The cw-diode laser (external cavity InGaAsP diode, Radians Innova) provides a few mW output in the 7465 cm^{-1} to 8025 cm^{-1} region in single frequency mode with a stability close to the intrinsic line width of 150 kHz on a ms time scale, and better than 1 MHz if it is locked to an external étalon. This corresponds thus to an effective instrumental resolving power of 2×10^8 near 7500 cm^{-1} . After an optical isolator which reduces unwanted back reflections, part of the laser output is diverted to external lock and monitor étalons. The main beam passes through an acousto-optical modulator (Isomet 1205C-2), and its first order deflection is coupled into a single mode optical fiber which transfers typically several 100 μW power to the ring-down cavity within a vacuum chamber. Light is coupled into the cavity using a lens to match the geometry of the laser beam to the single transversal Gaussian cavity mode TEM_{00} . The cavity is composed of two highly reflective concave mirrors with 1 m radius (Newport SuperMirrors, $R \geq 99.97\%$) mounted on an optical bench (Spindler & Hoyer, Mikrobank) at a distance $l = 32\text{ cm}$ in a linear stable resonator configuration. A solenoid nozzle^{37,40,41} with a $33 \times 0.1\text{ mm}$ slit generates pulsed supersonic jet expansions with $\approx 1.2\text{ ms}$ duration. To reduce Doppler broadening due to divergence of the gas pulse, the slit has been carefully aligned along the optical axis of the cavity. The probe distance between the nozzle orifice and the laser beam is 2 cm. The pump system (8000 l/s oil diffusion pump backed by a vacuum blower with a mechanical roughing pump) maintains a background pressure below $3 \times 10^{-4}\text{ mbar}$ in the vacuum chamber at 1 bar stagnation pressure and 10 Hz repetition rate of the nozzle. For room-temperature measurements, the chamber is filled with the sample gas (without pumps operating), and high precision gauges with temperature stabilization are used for measuring the sample pressure inside the chamber (Baratron capacitance gauges). The laser frequency reading is linearised during a scan employing the fringes of a 500 MHz monitor étalon, which is enclosed in an evacuated box. Its has a free spectral range of $0.017\ 127\ 573\text{ cm}^{-1}$, and the frequency drift is less than 1 MHz per day. The étalon is calibrated to absolute frequency reading by recording absorption spectra of HF vapor or CRD spectra of water vapor.^{42,43} After calibration, the CRD spectra have an estimated absolute wave number accuracy of 0.001 cm^{-1} .

One of the cavity mirrors is mounted on a piezoelectric transducer, to which a periodical triangular shaped voltage is applied to modulate the cavity length at a frequency of 20 Hz with an amplitude, which corresponds to slightly more than one free spectral range of the laser frequency. The cavity is thus twice in resonance with the laser during one period. In resonance, the cavity length is matched to the laser wavelength and the transmitted light intensity after the cavity increases suddenly. The resonance during the first half of one period is used to predict when a resonance in the first half of the *following* period will occur. At a given delay, the solenoid valve is then activated before the expected resonance, and in the maximum of the ensuing gas pulse a time window of 300 μs is defined. If the expected resonance occurs during that time window, it triggers the acousto-optical switch and the data acquisition. Since the pulsed nozzle is activated once

every second period, it has a 10 Hz repetition rate. Resonances occurring while the nozzle is not activated are collected separately to obtain the spectral baseline during the same scan, which saves time and also reduces noise sources by baseline drifts. Further aspects of this simple, but effective mode-matching scheme applicable to pulsed supersonic expansions are found in Ref. 37.

A fast InGaAs photodetector (NewFocus, 125 MHz) is used to observe the time-dependent intensity after the ring-down cavity. A sudden increase of the intensity over a certain threshold indicates the resonance condition. The acousto-optical modulator then switches-off the laser output, and the following exponential decay of intensity is stored into one of two digital oscilloscopes (Tektronix TDS 220, bandwidth reduced to 20 MHz), depending on whether it corresponds to a gas pulse absorption or to the background. To increase the signal to noise ratio, the signal bandwidth is further reduced to 2 MHz with an electronic Butterworth/Bessel filter (Model 3945, Krohn Hite) without effecting the time constant of the cavity decay. Several decay functions are averaged in the oscilloscopes and then transferred to a computer, which determines the ring-down constant k by fitting a single exponential function to the decay curve,

$$I(t) = \text{const} + I_0 \exp(-kt). \quad (3)$$

Cavity ringdown spectra of the absorbing species in the gas pulse and of the background are obtained simultaneously by scanning the laser frequency and measuring the corresponding decay time constants. The $1/e$ -decay time of the empty cavity is typically $\tau \approx 8 \mu\text{s}$, corresponding to a cavity quality factor $Q \approx 1 \times 10^{10}$ and a cavity finesse $F \approx 50\,000$. After $8 \mu\text{s}$, light has made 7500 passes in the cavity and has traveled 2.4 km, which is a measure for the effective absorption length.

Methane CH_4 ($\geq 99.5\%$, Pan Gas) was used without further purification for the jet experiments. For the room temperature measurements, it was purified by trap-to-trap distillation and repeated freeze-pump-thaw cycles, and it was in addition dried over phosphoric anhydride. FTIR spectra at room temperature were taken on our high-resolution FTIR spectrometer (BOMEM DA002), where the 2.5 m optical path difference allows a best instrumental resolution of 0.0024 cm^{-1} without apodization (with Hamming apodization 0.004 cm^{-1}), which is, however, not quite achieved near 7500 cm^{-1} .^{1,7,9,13} With a Doppler width $\Delta\tilde{\nu} = 0.023 \text{ cm}^{-1}$ [full width at half maximum (FWHM)] of room-temperature transitions of methane near 7510 cm^{-1} , an instrumental bandwidth of 0.01 cm^{-1} with Hamming apodization was chosen for the FTIR spectra displayed, corresponding to an effective instrumental resolving power near 700 000. In the $6500\text{--}8000 \text{ cm}^{-1}$ spectral region, the spectrometer was equipped with a halogen light source, a quartz beam splitter and a liquid nitrogen-cooled InSb detector. To increase sensitivity, the spectrometer was employed with a multipass White cell with 1.37 m base length (Portmann Instruments), which had an effective absorption path length of 30 m. Between about $6700\text{--}7450 \text{ cm}^{-1}$, water absorptions are apparent in the methane FTIR spectra due to water traces present, which were used for an *in situ* wave number calibration.⁴³

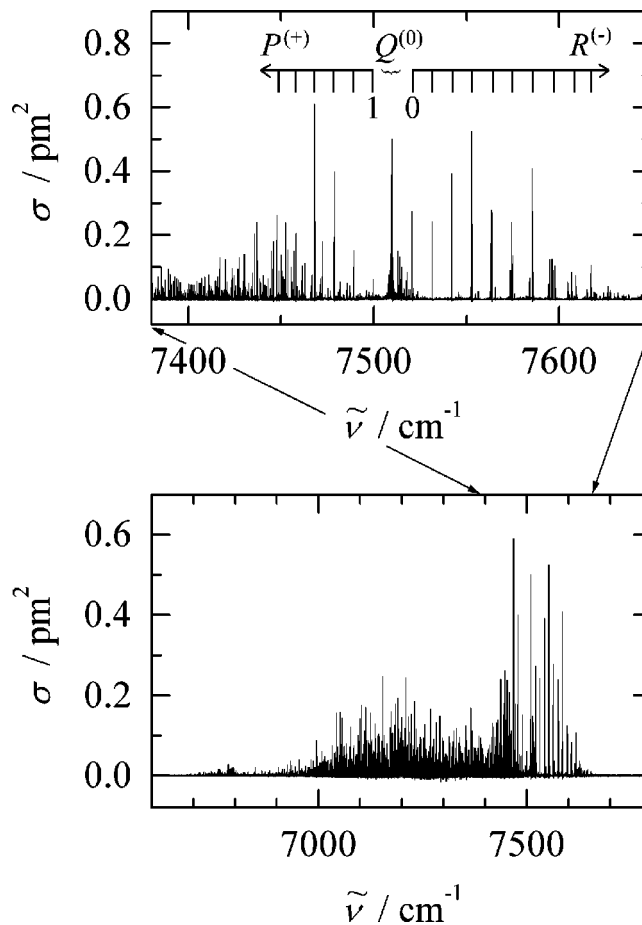


FIG. 1. Doppler-limited room temperature FTIR spectrum of the $N=2.5$ polyad (icosad) of methane (5.25 mbar) recorded in a 30 m multipass cell with an instrumental bandwidth of 0.01 cm^{-1} (FWHM, Hamming apodization). The upper panel shows enlarged the $\nu_2 + 2\nu_3$ combination band, which is part of the icosad (see text for details of the P , Q , and R assignment shown in the upper panel).

The absolute wavenumber accuracy should be about 0.001 cm^{-1} similar to the CRD spectra or slightly less accurate. In the methane FTIR spectra displayed below, water impurity lines have been subtracted using a water reference spectrum recorded under similar conditions.

III. RESULTS AND DISCUSSION

A. Survey of the polyad components

Methane $^{12}\text{CH}_4$ is a spherical top molecule belonging to the cubic point group T_d with four normal vibrations: ν_1 , the symmetric CH-stretching vibration (A_1 symmetry) observed at 2916.50 cm^{-1} , ν_2 , a CH-bending vibration (E symmetry) at 1533.33 cm^{-1} , ν_3 , the CH-stretching vibration (F_2 symmetry) at 3019.49 cm^{-1} , and ν_4 , a CH-bending vibration (F_2 symmetry) at 1310.76 cm^{-1} .^{30–32} Vibrations of E symmetry are doubly degenerate, and vibrations of F symmetry triply degenerate. Only F_2 vibrational bands are infrared active with allowed electric dipole transitions from the A_1 ground state.

Methane shows distinct rovibrational absorptions in the $6600\text{--}7700 \text{ cm}^{-1}$ region (Fig. 1), which are presumably largely due to overlapping vibrational bands of the $N=2.5$

TABLE I. Symmetry species in the groups T , T_d , S_4^* and the associated total nuclear spin I and Pauli-allowed rovibrational species for $^{12}\text{CH}_4$.

$\Gamma(T)$	$\Gamma(T_d)$	$\Gamma(T_d)\uparrow S_4^*$	([partition] ^{parity})	I	(Pauli allowed)
A	A_1	$A_1^+ + A_2^-$	([4] ⁺ + [1 ⁴] ⁻)	2	(A_2^-)
A	A_2	$A_2^+ + A_1^-$	([1 ⁴] ⁺ + [4] ⁻)	2	(A_2^+)
E	E	$E^+ + E^-$	([2 ²] ⁺ + [2 ²] ⁻)	0	($E^+ + E^-$)
F	F_1	$F_1^+ + F_2^-$	([2,1 ²] ⁺ + [3,1] ⁻)	1	(F_1^+)
F	F_2	$F_2^+ + F_1^-$	([3,1] ⁺ + [2,1 ²] ⁻)	1	(F_1^-)

polyad.³⁷ The $N=2.5$ polyad is composed of 20 overtone and combination bands (icosad), but no definitive assignment exists at present. In its high wave number region, regularly spaced lines are apparent (Fig. 1), which have been assigned to the $\nu_2 + 2\nu_3$ combination band in 1933.⁴⁴ This assignment, however, has not been confirmed yet. At the low resolution, which was then available, a spectral assignment seemed to be rather straightforward: All Q -branch transitions merge to one single line near 7510 cm^{-1} , and a progression of regularly spaced P - and R -branch lines can be easily followed from $P(1)$ to $P(6)$ and from $R(0)$ to $R(10)$. More recently, this spectral region has also been measured at medium resolution at 77 K in the gas phase (0.14 cm^{-1} FWHM, Ref. 45) and in liquid argon solutions (95 K),⁴⁶ but without providing a more detailed analysis.

Combinations with two CH-stretching and one CH-bending vibrational quanta are chromophore states in the $N=2.5$ polyad in a zeroth-order description. Other bands gain their intensity mainly by mixing with chromophore states. The band in the high wave number region has the strongest peak intensities within the polyad. It is therefore reasonable to assume that it approximately belongs to a chromophore transition. Among them, $\nu_2 + 2\nu_3$ is highest in energy. Taking the sum of the observed positions of ν_2 (Ref. 32) and $2\nu_3$ (Ref. 47) as an estimate for $\nu_2 + 2\nu_3$ and adding $6G_{33} - 8T_{33} - 8T_{23} \approx 33\text{ cm}^{-1}$ to take account of the subband splitting⁴⁸ (details see below), 7535 cm^{-1} is then the estimated position of the IR-active F_2 component of $\nu_2 + 2\nu_3$. Since anharmonicities have been neglected, this estimation will be slightly too high, and the observed position near 7510 cm^{-1} is thus in reasonable agreement with the proposed assignment. Other chromophore states would be $\nu_1 + \nu_2 + \nu_3$, about 100 cm^{-1} lower, and $2\nu_1 + \nu_2$ and $2\nu_3 + \nu_4$ expected around 7300 cm^{-1} .

The 12-fold vibrational degeneracy of the combination band $\nu_2 + 2\nu_3$ is distributed among its six vibrational subbands (components) of A_1 , A_2 , E , E , F_1 , and F_2 symmetry, which are all coupled by vibration-rotation interactions. Only the F_2 vibrational subband is IR-active in zeroth-order approximation, but other subbands also acquire IR intensity by mixing with the F_2 component. At low rotational energies and J -values, Coriolis interactions are not very effective, and the transitions to the $\nu_2 + 2\nu_3$ combination band will thus resemble a regular (unperturbed) F_2 -band [compare the discussion for $2\nu_3$ (Ref. 49)]. At higher J -values, the Coriolis perturbation will become more important, and a rovibrational analysis has then to include all components of the combination band.

B. Symmetry, selection rules, and nuclear spin isomers

The traditional symmetry assignment of rovibrational levels of methane uses the rotational subgroup T of the point group of the molecular equilibrium configuration, which is sufficient for describing nuclear spin isomers and nuclear spin statistical weights. It has been known for some time though, that the full T_d point group species can be employed as well.^{50–52} In addition, when inversion or “stereomutation”¹⁴ is considered, one can use the full permutation inversion group S_4^* following Longuet-Higgins.^{25,52,53}

For convenience, Table I summarizes the situation, using the systematic nomenclature of Ref. 25 which assigns well-defined permutation group species in the symmetric group S_4 ($A_1 \equiv [4]$, $A_2 \equiv [1^4]$, $E \equiv [2^2]$, $F_1 \equiv [2,1^2]$, $F_2 \equiv [3,1]$, see Refs. 25, 54 for the partition notation) and parity (+ or -) in the inversion group $S^* \equiv \{E, E^*\}$. S_4^* is the direct product of S_4 and S^* . For the four protons in CH_4 the spin functions are of symmetry species A_1 for total nuclear spin $I=2$, F_2 for $I=1$, and E for $I=0$ in S_4 . The total Pauli allowed species are the totally antisymmetric A_2 in S_4 (and A_2^+ and A_2^- in S_4^*) and thus we obtain the combinations of nuclear spin functions with Pauli-allowed rovibrational species as shown in Table I. It is clear from Table I that A_1 , A_2 , F_1 , and F_2 levels in T_d have a well defined parity and permutation symmetry in S_4^* , whereas E in T_d corresponds to a closely degenerate doublet E^+ and E^- in S_4^* . Effective nuclear spin weights are thus $g_I=5$ for A -levels, $g_I=2$ for E -levels, and $g_I=3$ for F -levels. The frequency of occurrence M of T_d species for a given J has been given by Ref. 55 in the form of equations and in Ref. 56 in general tabular form. Since Ref. 55 contains nontrivial misprints, the corrected equations are reproduced below for convenience,

$$\begin{aligned}
 24M(J, A, \rho) &= 2J + 1 + 3(-1)^J + (-1)^{\rho+J} [6 + g_1(J)] \\
 &\quad + g_2(J), \\
 24M(J, E) &= 4J + 2 + 6(-1)^J - g_2(J), \\
 24M(J, F, \rho) &= 6J + 3 - 3(-1)^J + (-1)^{\rho+J} [6 - g_1(J)],
 \end{aligned} \tag{4}$$

with auxiliary functions $g_1(J) = 6(-1)^J [\sin(\frac{1}{2}J\pi) + \cos(\frac{1}{2}J\pi)]$ and $g_2(J) = 8[3^{-1/2} \sin(\frac{2}{3}J\pi) + \cos(\frac{2}{3}J\pi)]$. $\rho=1$ for A_2 or F_1 , and $\rho=2$ for A_1 or F_2 .

The triply degenerate F_2 vibrational level has three components, denoted $F^{(-)}$, $F^{(0)}$, and $F^{(+)}$, which are coupled by

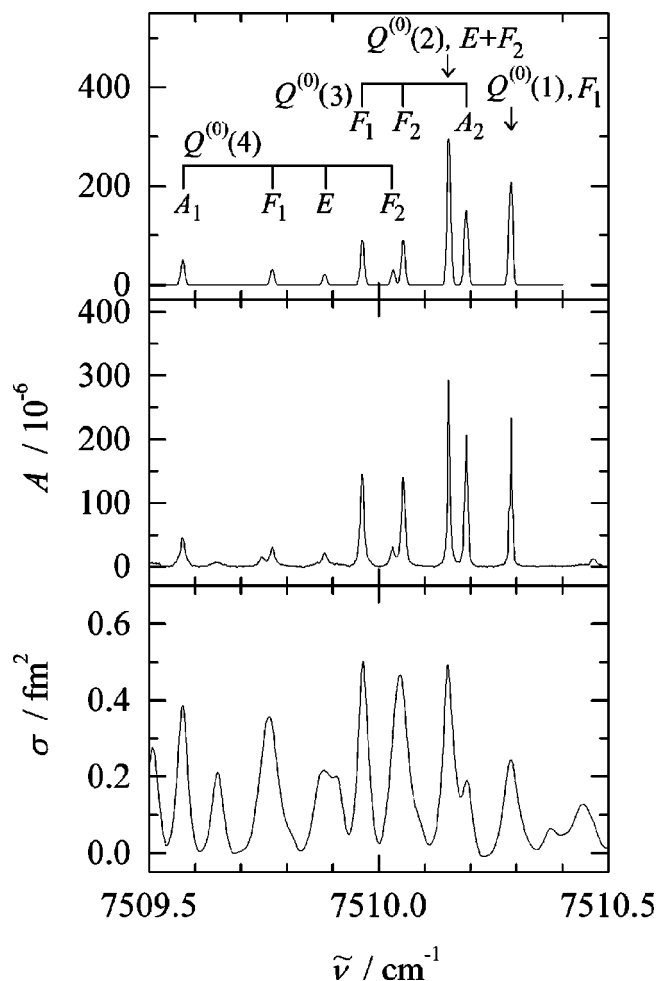


FIG. 3. Q -branch region of the $\nu_2 + 2\nu_3$ combination band of $^{12}\text{CH}_4$. Lower panel: Doppler-limited FTIR spectrum at room temperature (conditions as in Fig. 1); middle panel: cw-CRD spectrum of a slit jet expansion of 1 bar methane; upper panel: simulated spectrum corresponding to a rotational temperature of 45 K (see text for details).

metry “conserved” distribution⁷ is derived similar to Eq. (6), except that p_i has in addition to be multiplied by the corresponding mole fraction x of the nuclear spin isomer at room temperature, and the summation in the rotational partition function Q_{rot} extends only over the allowed rotational levels of the corresponding isomer.

C. Assignment of the rovibrational line spectra

In the present work, the Q -branch region of $\nu_2 + 2\nu_3$ around 7510 cm^{-1} , and also some selected P - and R -branch lines have been recorded employing cw-CRD in a pulsed slit jet expansion of 1 bar methane and combined with the Doppler-limited FTIR spectra at room temperature. Figure 3 shows the Q -branch region of $\nu_2 + 2\nu_3$. The Doppler width of the rotationally resolved transitions decreases from $\Delta\tilde{\nu} = 0.0233\text{ cm}^{-1}$ (FWHM) at room temperature to 0.0098 cm^{-1} in the slit jet expansion, which corresponds to 54 K as a formal Doppler temperature. It is clearly evident from Fig. 3 that rotational cooling in the jet expansion simplifies the spectrum and improves the spectral resolution; this is a prerequisite for an assignment of the congested Q -branch.

The scalar rovibrational term values of an F -vibrational level are approximately given by Eq. (9), where centrifugal distortion and tetrahedral splitting of rotational levels have been neglected,

$$F^{(+)}(J) = \nu_0 + B_v J(J+1) + 2B_v \zeta_v J,$$

$$F^{(0)}(J) = \nu_0 + B_v J(J+1) - 2B_v \zeta_v, \quad (9)$$

$$F^{(-)}(J) = \nu_0 + B_v J(J+1) - 2B_v \zeta_v (J+1),$$

where ζ_v is the Coriolis interaction parameter.^{48,57} B_v is an effective rotational constant with different values in the $F^{(0)}$ and $F^{(\pm)}$ subsystems.^{48,49} ν_0 is the vibrational origin; it corresponds to the term value of the lowest quantum level, $F^{(+)}(0)$. In the lowest order of approximation, the tetrahedral splitting of a rotational level J is proportional to the Clebsch–Gordan coefficient $F_{A_1,pp}^{(4RR)}$, where $R = (J+1)$, J and $(J-1)$ for $F^{(+)}$, $F^{(0)}$, and $F^{(-)}$, respectively, and where p labels the rotational symmetry species.^{60,61,74} A linear fit of the term values of tetrahedrally split components versus the corresponding $F_{A_1,pp}^{(4RR)}$ coefficients therefore yields as slope the proportionality factor and as intercept the scalar term value of the rotational level. Equation (9) holds for an isolated fundamental band, with one quantum of the triply degenerate F -vibration excited. Vibrational overtone and combination bands (as $\nu_2 + 2\nu_3$) split into components (subbands) of different symmetry, which are mixed by Coriolis interactions. An isolated band description of term values as in Eq. (9) is then approximately valid provided that the perturbations are not very effective.⁴⁹

With tabulated ground state term values⁶² and the above, simple expressions for excited state term values, transition energies can be calculated. Using these values and, furthermore, line strengths (see below) as guidance, it was rather straightforward to assign the low-lying lines in the R - and P -branches observed in high-resolution room-temperature FTIR and slit jet cw-CRD spectra. All components of $R^{(-)}(0)$ to $R^{(-)}(3)$ and $P^{(+)}(1)$ to $P^{(+)}(3)$ could thus be determined (J -values in parentheses). The Q -branch at room temperature, however, is very congested, since components of different rotational levels are overlapping. Jet cooling was in this case essential to identify the low-lying lines of the Q -branch, from $Q^{(0)}(1)$ to $Q^{(0)}(4)$. In this notation, the superscript $(-)$, (0) or $(+)$ denotes a transition to the $F^{(-)}$, $F^{(0)}$ or $F^{(+)}$ -component, respectively. Since the strongly allowed P , Q , and R -branches terminate in different components of the F -vibrational state, the method of identifying “combination differences,”⁵⁷ which often greatly facilitates the assignment of rotationally resolved IR spectra, is not very useful in the present case. In the upper panel of Fig. 3, a simulation of the Q -branch transitions is shown assuming a nuclear spin symmetry conserving rotational distribution at 45 K. The agreement between the simulation and the jet experiment is very satisfactory, which supports the assignment. The assigned rovibrational transitions of $\nu_2 + 2\nu_3$, transition energies and term values are finally summarized for convenience in Table II. In J -levels with several F -components, the order of the sequence of F -components cannot be decided with intensity arguments. In the assign-

TABLE II. Assigned transitions from the ground state and term values for $\nu_2+2\nu_3$ of $^{12}\text{CH}_4$. (a) The $F^{(-)}$ sublevel of $\nu_2+2\nu_3$. (b) The $F^{(0)}$ sublevel of $\nu_2+2\nu_3$. (c) The $F^{(+)}$ level of $\nu_2+2\nu_3$.

Transition	$\Gamma(T_d)$	$\bar{\nu}/\text{cm}^{-1a}$	Lower state ^b	Term values/ cm^{-1}	
				Upper state	
(a)					
$R^{(-)}(0)$	A_1	7520.8565	0	7520.8565	
$R^{(-)}(1)$	F_1	7531.4174	10.481649	7541.8990	
$R^{(-)}(2)$	E, F_2^c	7542.0682	31.4422 ^c	7573.5104	
$R^{(-)}(3)$	A_2	7552.7361	62.878173	7615.6143	
	F_2	7552.8059	62.876845	7615.6827	
	F_1	7552.9779	62.875783	7615.8537	
				7615.752(32)/-0.6(2) ^d	
(b)					
$Q^{(0)}(1)$	F_1	7510.2873	10.481649	7520.7689	
$Q^{(0)}(2)$	E, F_2^c	7510.1531	31.4422 ^c	7541.5953	
$Q^{(0)}(3)$	A_2	7510.1902	62.878173	7573.0684	
	F_2	7510.0533	62.876845	7572.9301	
	F_1	7509.9636	62.875783	7572.8394	
				7572.912(6)/0.62(3) ^d	
$Q^{(0)}(4)$	F_2	7510.0309	104.78002	7614.8109	
	E	7509.8820	104.77604	7614.6580	
	F_1	7509.7682	104.77471	7614.5429	
	A_1	7509.5727	104.77285	7614.3456	
				7614.631(34)/-1.4(3) ^d	
(c)					
$P^{(+)}(1)$	F_1	7499.8562	10.481649	7510.3378	
	F_2	7489.3359	31.442389	7520.7783	
$P^{(+)}(2)$	E	7489.2936	31.442123	7520.7357	
					7520.761/-0.14 ^d
$P^{(+)}(3)$	A_2	7479.0013	62.878173	7541.8795	
	F_2	7478.7163	62.876845	7541.5931	
	F_1	7478.6296	62.875783	7541.5054	
				7541.603(39)/1.0(2) ^d	

^aGaussian line profile fits with 0.001 cm^{-1} estimated uncertainty, for P - and R -lines to room-temperature FTIR spectra and for Q -lines to the cw-CRD-jet spectra.

^bFrom Ref. 62.

^c E and F_2 -components not resolved. For the ground state, a mean term value was chosen.

^dScalar term value/proportionality factor from a linear fit of tetrahedral splittings vs the corresponding $F_{A_1PP}^{(4RR)}$ coefficients (see text). In parentheses are standard deviations in the unit of the last figure quoted, except for $P^{(+)}(2)$. The values given below the horizontal lines correspond to a weighted average of those term values given just above it, which relate to the same value of J .

ment of tetrahedral splittings, the order is consistent with the sequence of the $F_{A_1PP}^{(4RR)}$ coefficients.^{60,61} The scalar term value and proportionality factor obtained from a linear fit of tetrahedral splittings versus the corresponding $F_{A_1PP}^{(4RR)}$ coefficients is also included in Table II.

As a further example of slit jet cw-CRD, Fig. 4 shows the $P^{(+)}(1)$ transition from the $J=1$ ground state level of ortho-methane and the two resolved components of $P^{(+)}(2)$ from the $J=2$ ground state levels of ortho- and para-methane. $J=2$ is the lowest quantum level for para-methane, while for ortho-methane also $J=1$ is allowed. In a nuclear spin symmetry conserving distribution, the intensity ratio of both $P(2)$ components thus allows a determination of the rotational temperature of the jet expansion.^{7,8} In the present case an estimate of about 40 K is obtained in agreement with the simulation of the jet-cooled Q -branch. The $P^{(+)}(1)$ transition terminates in the lowest quantum level of

the excited vibrational state, $F^{(+)}(0)$. With a measured transition at $7499.8562 \text{ cm}^{-1}$ and a known ground state term value of $10.481649 \text{ cm}^{-1}$,⁶² the term value of $F^{(+)}(0)$ is then $7510.3378 \text{ cm}^{-1}$ with an estimated uncertainty of 0.001 cm^{-1} . This value is the vibrational origin ν_0 of the combination band $\nu_2+2\nu_3$; it represents a benchmark for calculations of vibrational level positions.¹³⁻²²

D. Perturbations

The regular appearance of low-resolution spectra and the successful analysis and assignment of the low-lying rotational levels may create the impression that the combination band $\nu_2+2\nu_3$ can be treated as an isolated, regular F -band transition. A preliminary fit of rotational term values (Table II) to Eq. (9) yielded $\nu_0=7510.25(3) \text{ cm}^{-1}$, $\zeta_v=-0.006(2) \text{ cm}^{-1}$, and $B_v=5.216(1) \text{ cm}^{-1}$ for $F^{(0)}$ and $B_v=5.256(3) \text{ cm}^{-1}$ for $F^{(\pm)}$, where the values in parenthe-

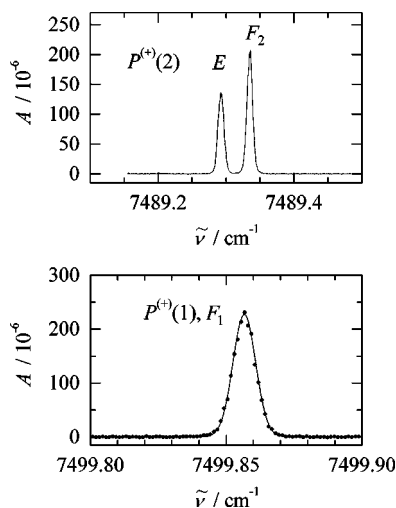


FIG. 4. P -branch transitions of the $\nu_2 + 2\nu_3$ combination band of $^{12}\text{CH}_4$, observed by cw-CRD spectroscopy in a slit jet expansion of 1 bar methane. Lower panel: $P^{(+)}(1)$ line (F_1 -component). The fit line is a Gaussian curve with $\Delta\tilde{\nu} = 0.00984(2) \text{ cm}^{-1}$ (FWHM), corresponding to a Doppler temperature of $T_{\text{Doppler}} = 53.7(2) \text{ K}$. Upper panel: Both components of the $P^{(+)}(2)$ line. The relative intensities of the E - and F_2 -components can be used as a thermometer for the rotational temperature (see text).

ses are estimated standard deviations in the units of the last figure quoted. Compared to the ground state value^{58,59} $B_0 = 5.24104 \text{ cm}^{-1}$, the effective rotational constants appear to be rather large (see also a related finding for $2\nu_3$ in Ref. 63). The parameters are presumably effected by perturbations and should be considered as fit parameters, only. With a standard deviation 0.07 cm^{-1} of the 11 calculated term values, the fit is not very satisfactory; this also indicates the presence of strong perturbations. On closer inspection of the spectra, it becomes obvious that higher rotational levels are heavily perturbed, with additional transitions and irregular intensities. An assignment of levels with $J=5$ and higher (rotational terms higher than 100 cm^{-1}) was thus not possible. Such an assignment must include also the perturbing vibrational states. As example, Fig. 5 shows the range of the $P(3)$ and $P(4)$ transitions of the $\nu_2 + 2\nu_3$ combination band of $^{12}\text{CH}_4$, observed by Doppler-limited Fourier transform infrared (FTIR) spectroscopy at room temperature. The three

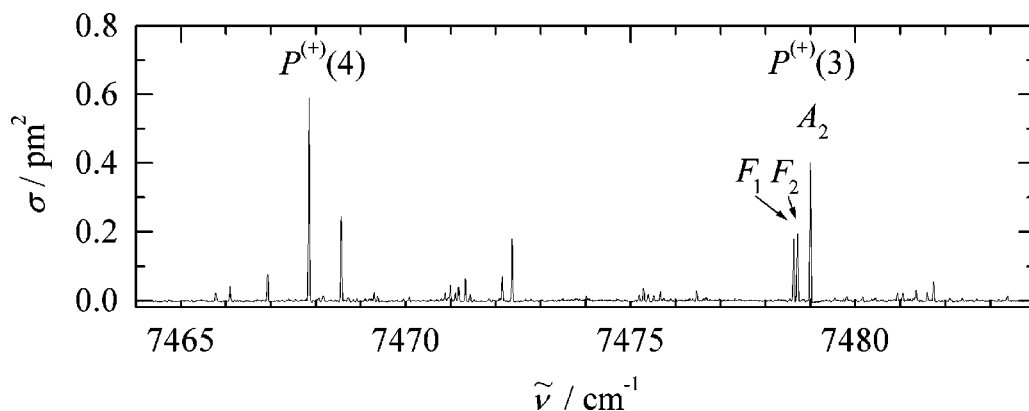


FIG. 5. P -branch transitions of the $\nu_2 + 2\nu_3$ combination band of $^{12}\text{CH}_4$, observed by FTIR spectroscopy at room temperature and Doppler-limited resolution (5.25 mbar methane, 30 m multipass cell, 0.01 cm^{-1} instrumental bandwidth FWHM, Hamming apodization).

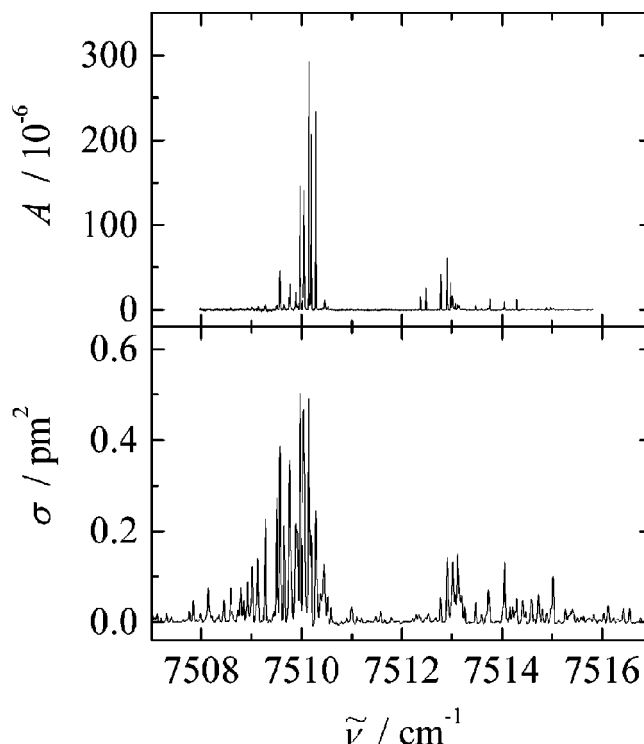


FIG. 6. Q -branch of the $\nu_2 + 2\nu_3$ combination band of $^{12}\text{CH}_4$ around 7510 cm^{-1} . The upper trace shows the cw-CRD slit jet spectrum of an expansion of 1 bar methane. For comparison, the lower trace shows the Doppler-limited room temperature FTIR spectrum of 5.25 mbar methane recorded in a 30 m multipass cell with 0.01 cm^{-1} instrumental bandwidth (FWHM, Hamming apodization).

components of $P^{(+)}(3)$ are easily assigned; they are the most dominant transitions in the expected region around 7479 cm^{-1} , and they have the expected intensity ratio. In the 7468 cm^{-1} region, however, the A_1 , F_1 , E , and F_2 components of a regular $P^{(+)}(4)$ transition would be expected with an approximate intensity ratio of 5:3:2:3, respectively, but this pattern is not found in the spectrum (Fig. 5). For both $P^{(+)}(3)$ and $P^{(+)}(4)$, additional transitions grouped around $3\text{--}4 \text{ cm}^{-1}$ higher in wave number are apparent, which become stronger compared to the “regular” transitions with increasing J . This could indicate perturbations due to a Co-

TABLE III. Symmetry splitting in some overtone and combination bands of a tetrahedral molecule and vibrational positions of methane.

State		Splitting term (following Ref. 48)	Observed position/cm ⁻¹
ν_2	E	G_{22}	1533.33 (Ref. 32)
$2\nu_3$	A_1	0	5968.1 (Ref. 63)
	E	$6G_{33}+12T_{33}$	6043.8 (Ref. 65)
	F_2	$6G_{33}-8T_{33}$	6004.99 (Ref. 47)
$\nu_2+\nu_3$	F_2	$G_{22}+2G_{33}+8T_{23}$	4543.76 (Ref. 66)
	F_1	$G_{22}+2G_{33}-8T_{23}$	4537.57 (Ref. 66)
$\nu_2+2\nu_3$	A_1	$G_{22}+6G_{33}+12T_{33}+16T_{23}$	7559 ^a
	A_2	$G_{22}+6G_{33}+12T_{33}-16T_{23}$	7546 ^a
	F_1	$G_{22}+6G_{33}-8T_{33}+8T_{23}$	7516.5 ^a
	F_2	$G_{22}+6G_{33}-8T_{33}-8T_{23}$	7510.3378 ^b
	E	$G_{22}+3G_{33}+6T_{33}+\sqrt{(3G_{33}+6T_{33})^2+256T_{23}^2}$	7553 ^a
	E	$G_{22}+3G_{33}+6T_{33}-\sqrt{(3G_{33}+6T_{33})^2+256T_{23}^2}$	7476 ^a

^aCalculated, using the shift relative to the observed position of the F_2 -component.

^bPresent work.

riolis resonance. Figure 6 shows as a further example the spectral region around the Q -branch of $\nu_2+2\nu_3$, observed by room-temperature FTIR and cw-CRD spectroscopy in a supersonic slit-jet expansion. The rovibrational lines around 7510 cm⁻¹ are assigned to the regular F_2 Q -branch. The additional lines grouped around 7513 cm⁻¹ cannot presently be assigned; they are indicative of a resonance. The nature and identity of the relevant perturbing states is unknown, but it would be very reasonable to assume that the various symmetry components of $\nu_2+2\nu_3$ interact very strongly by Coriolis resonances, which become more effective with higher J -values. Such interactions have been observed before in all lower polyads of methane, for example in the $2\nu_3$ and $2\nu_4$ bands,⁴⁹ where the interaction between the E - and F_2 -component has to be considered, or in $\nu_2+\nu_3$,⁶⁴ where the F_1 and F_2 -vibrational components are strongly interacting. In all these cases and presumably also in the present combination band, an isolated band analysis of the F_2 -component can only be an approximation valid for low J -values.

Using perturbation theory, Hecht has derived expressions for the symmetry splitting of various combination bands of tetrahedral molecules (see Table III).⁴⁸ The coefficients are, in the corresponding order of theory, functions of potential terms of methane,⁴⁸ but it is probably more practical to consider them as effective parameters, which can be obtained from a fit to observed vibrational term values. To obtain the relative splitting in the combination band $\nu_2+2\nu_3$, the coefficients G_{33} , T_{33} , and T_{23} are required. $G_{33}\approx 8.7$ cm⁻¹ and $T_{33}\approx 2.0$ cm⁻¹ are obtained from the spacing of the $2\nu_3$ components,^{47,63,65} and $T_{23}\approx 0.4$ cm⁻¹ from the splitting of the F_1 - and F_2 -components in $\nu_2+\nu_3$ (Refs. 64, 66) (see Table III). With these coefficients and the observed vibrational origin of the F_2 -component, estimated vibrational positions of the symmetry components of $\nu_2+2\nu_3$ have been calculated; they are also listed in Table III. It can be seen that the F_1 -component is rather close to the IR-active F_2 -component; it is only about 6 cm⁻¹ higher in wave number, and analogous to $\nu_2+\nu_3$,⁶⁴ a strong interaction between

these components can be expected. It is thus very likely that additional transitions, which have been observed about 3 cm⁻¹ higher in wave number than the “regular” F_2 Q -branch, are due to the F_1 -component, which gains intensity by Coriolis interaction and mixing with F_2 . In addition, further Coriolis resonances and anharmonic resonances with other members of the $N=2.5$ icosad system may also be effective. A more extensive rovibrational analysis of $\nu_2+2\nu_3$ including these perturbations is in progress.

E. Line strengths and integrated band strength

The integrated vibrational band strength,

$$G = \int_{\text{band}} \sigma(\nu) d \ln \nu, \quad (10)$$

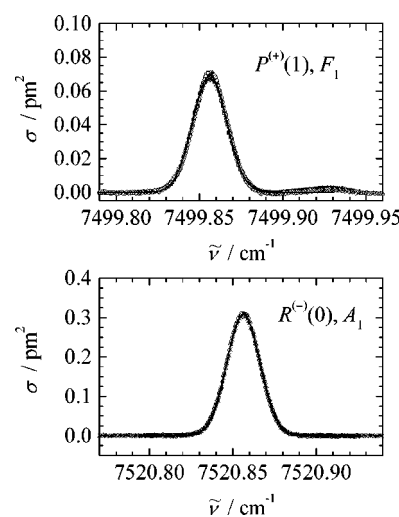


FIG. 7. Absorption cross sections of $R^{(-)}(0)$, A_1 (lower panel) and $P^{(+)}(1)$, F_1 (upper panel) of $\nu_2+2\nu_3$ of $^{12}\text{CH}_4$ obtained by cw-CRD at 299 K. Data points for the $R(0)$ -line represent two independent measurements at 0.022 and 0.024 mbar sample pressures, and for the $P(1)$ -line four measurements between 0.08 and 0.28 mbar. The fit lines are Gaussians corresponding to effective Doppler temperatures of 299 ± 3 and 319 ± 12 K for the R - and P -line, respectively (uncertainties estimated from the scatter of single data sets).

is a very characteristic property of a vibrational transition.^{1,15,67} G is defined as the integrated absorption cross section over all rotational transitions belonging to the band, making appropriate corrections for vibrational level populations and stimulated emission, if necessary. If it is known, the absolute intensities of rovibrational lines at any temperature can be calculated, and concentrations of the absorbing species can be evaluated. The integrated band strength also allows the determination of the vibrational transition moment $|\mu_v|$ that can be compared with *ab initio* calculations of dipole moment functions.^{1,13,15,18,67,68} For the triply degenerate vibration, the integrated band strength G is related to the vibrational transition moment via Eq. (11),^{67,69,70}

$$G = \frac{1}{4\pi\epsilon_0} \frac{8\pi^3}{3hc} 3|\mu_v|^2 = 124.87(|\mu_v|/D)^2 \text{ pm}^2, \quad (11)$$

where the first part is in SI units. In the second part, the constants have been inserted with the vibrational transition moment $|\mu_v|$ in the unit D (Debye).

The integrated absorption strength G_{fi} of a rovibrational absorption line from the initial lower state i to a final excited state f is approximately given by Eq. (12),^{67,69,70}

$$G_{fi} = \int_{\text{line}} \sigma(\nu) d \ln \nu = p_i G R_{fi} F d. \quad (12)$$

p_i is the fractional population of the ground state, G is the vibrational band strength, and F is a factor similar to the Herman–Wallis factor for diatomic molecules. It is empirically given as $F = 1 + \alpha_1 m + \alpha_2 m^2 + \dots$, where $m = -J_i, 0$, and $J_i + 1$ for P , Q , and R -branches, respectively.^{71–73} F considers the transformation of the dipole moment operator due to rotation–vibration interactions. d takes account of the dilution of line strength by admixing dark state character by Coriolis interactions. At low J values, Coriolis interactions are not very effective; F and d are then close to 1 and can be neglected. R_{fi} is the rotational line strength factor for the $F_2 \leftarrow A_1$ transition,^{67,69,70}

$$R_{fi} = \frac{1}{3} \frac{2J_f + 1}{2J_i + 1}. \quad (13)$$

cw-CRD spectroscopy at room temperature has been employed to measure very accurately the integrated absorption cross sections of selected rovibrational transitions of the $\nu_2 + 2\nu_3$ combination band under well-defined temperature and sample pressure conditions; this corresponds to the determination of G_{fi} . The result has then been extrapolated to the total integrated vibrational band strength G using calculated populations p_i . A direct integration over all rovibrational lines of $\nu_2 + 2\nu_3$ might introduce systematic errors, since many transitions in the range of the combination band belong to other members of the polyad $N = 2.5$. Nevertheless, in order to provide an estimate independent from the cw-CRD measurements, such a direct integration was performed on the room-temperature FTIR spectrum (Fig. 1), giving $G = 1.22 \times 10^{-4} \text{ pm}^2$ (integration from 7400 to 7650 cm^{-1}). The cw-CRD measurements are performed for transitions with low J_f values, which are not effected much by Coriolis

interactions. The extrapolation thus allows the determination of the *unperturbed* vibrational transition moment of $\nu_2 + 2\nu_3$.

Figure 7 shows the absorption cross sections of $R^{(-)}(0)$ and $P^{(+)}(1)$ of $\nu_2 + 2\nu_3$ of $^{12}\text{CH}_4$ obtained by cw-CRD spectroscopy at a measured temperature of $299 \pm 1 \text{ K}$ and at different sample pressures ranging from 0.022 to 0.28 mbar. The data points are well represented by Gaussians corresponding to a room-temperature Doppler width. For $R^{(-)}(0)$, an integrated rovibrational line strength of $G_{fi} = (1.03 \pm 0.02) \times 10^{-6} \text{ pm}^2$ is obtained, and for $P^{(+)}(1)$, $G_{fi} = (0.237 \pm 0.003) \times 10^{-6} \text{ pm}^2$. The estimated uncertainties are dominated by the uncertainty of the sample pressure measurement. With a calculated rotational partition function $Q_{\text{rot}} = 595.8$ at 299 K, the population of the $J_i = 0$ ground state level (A_1 -symmetry) is $p_i = 0.00839$. $J_i = 1$ (F_1 -symmetry) has a rotational term value of 10.48 cm^{-1} and $p_i = 0.01436$. Using Eq. (12), an integrated band strength G of $1.21 \times 10^{-4} \text{ pm}^2$ from the $R(0)$ -line and $1.48 \times 10^{-4} \text{ pm}^2$ from the $P(1)$ -line is extrapolated, giving a combined value $G = 1.34 \times 10^{-4} \text{ pm}^2$ with about 10% uncertainty, which is in excellent agreement with the FTIR estimate. With Eq. (11), a vibrational transition moment $|\mu_v| = 1.04 \times 10^{-3} \text{ D}$ is then evaluated with about 3% uncertainty (the sign is undetermined). Combining the cw-CRD with the FTIR data and allowing for various systematic uncertainties, we may quote as a final estimate $G = (1.3 \pm 0.2) \times 10^{-4} \text{ pm}^2$ and $|\mu_v| = (1.0 \pm 0.1) \times 10^{-3} \text{ D}$. Previously, $|\mu_v| = 0.0534(3) \text{ D}$ has been determined for the fundamental ν_3 .⁶⁷ The combination band $\nu_2 + 2\nu_3$ is thus about 3000 times weaker (for the ratios of G), which is within expectation. The experimental band strength values are necessary for modeling intensities in $\nu_2 + 2\nu_3$ and for analytical applications. They also represent benchmarks for *ab initio* calculations.^{16–21}

IV. CONCLUSIONS

The complex rovibrational spectrum of methane between 6600 and 7700 cm^{-1} is a typical example, where an IR spectrum contains rich information about the anharmonic potential and dipole moment functions. The absorptions are due to the $N = 2.5$ icosad of methane, and the $\nu_2 + 2\nu_3$ combination band at its high-wave-number region near 7510 cm^{-1} was studied here in detail both by FTIR spectroscopy at room temperature and Doppler-limited resolution and by cw-CRD spectroscopy at room temperature and in a supersonic slit jet expansion. The increased spectral resolution due to the reduced Doppler width of rovibrational transitions in the slit jet and the spectral simplification afforded by the rotational cooling of the supersonic expansion allowed for an assignment of the transitions at low J -values. The vibrational origin of $\nu_2 + 2\nu_3$ at 7510.3378 cm^{-1} , the integrated band strength $G = 1.3 \times 10^{-4} \text{ pm}^2$ and the vibrational transition moment $|\mu_v| = 1.0 \times 10^{-3} \text{ D}$ have been determined. The values represent benchmarks to test the quality of effective vibrational Hamiltonians and *ab initio* potentials and dipole moment functions.^{15,16} Although an isolated band analysis is possible at low J -values, the influence of strong perturbations becomes evident at higher rotational excitation. The

F_1 -component of $\nu_2 + 2\nu_3$ interacting by a strong Coriolis coupling with the IR-active F_2 -component appears to be a dominant perturber. A more detailed rovibrational analysis extending to higher J -values and including perturbing states is in progress, with the ultimate aim of a complete rovibrational analysis of the $\nu_2 + 2\nu_3$ combination band and eventually of the entire $N=2.5$ icosad of methane. The present study demonstrates that cw-CRD spectroscopy in pulsed supersonic slit jet expansions is a powerful new tool in infrared spectroscopy, particularly also when combined with large, but frequently unassigned, data sets available from high-resolution FTIR spectroscopy.

ACKNOWLEDGMENTS

The authors are grateful to Hans Hollenstein for help and discussions. This work is supported financially by the ETH Zürich (including C4 and CSCS), the Schweizerischer Nationalfonds, and the AGS project.

- ¹M. Quack, *Annu. Rev. Phys. Chem.* **41**, 839 (1990).
- ²K. K. Lehmann, G. Scoles, and B. H. Pate, *Annu. Rev. Phys. Chem.* **45**, 241 (1994).
- ³M. Quack, in *Femtosecond Chemistry*, edited by J. Manz and L. Wöste (VCH, Weinheim, 1995), Chap. 27, pp. 781–818.
- ⁴L. Lubich, O. V. Boyarkin, R. D. F. Settle, D. S. Perry, and T. R. Rizzo, *Faraday Discuss.* **102**, 167 (1995).
- ⁵D. J. Nesbitt and R. W. Field, *J. Phys. Chem.* **100**, 12735 (1996).
- ⁶M. Gruebele and R. Bigwood, *Int. Rev. Phys. Chem.* **17**, 91 (1998).
- ⁷A. Amrein, M. Quack, and U. Schmitt, *J. Phys. Chem.* **92**, 5455 (1988).
- ⁸R. Georges, M. Herman, J.-C. Hilico, and O. Robert, *J. Mol. Spectrosc.* **187**, 13 (1998).
- ⁹M. Lewerenz and M. Quack, *J. Chem. Phys.* **88**, 5408 (1988).
- ¹⁰(a) T. Carrington, Jr., L. Halonen, and M. Quack, *Chem. Phys. Lett.* **140**, 512 (1987); (b) L. Halonen, T. Carrington, Jr., and M. Quack, *J. Chem. Soc., Faraday Trans. 2* **84**, 1371 (1988); (c) L. Halonen, *J. Chem. Phys.* **106**, 831 (1997).
- ¹¹L. Wiesenfeld, *J. Mol. Spectrosc.* **184**, 277 (1997).
- ¹²R. Lemus and A. Frank, *J. Mol. Spectrosc.* **201**, 198 (2000).
- ¹³H. Hollenstein, R. Marquardt, M. Quack, and M. A. Suhm, *J. Chem. Phys.* **101**, 3588 (1994).
- ¹⁴M. J. M. Pepper, I. Shavitt, P. v. Ragué Schleyer, M. N. Glukhovtsev, R. Janoschek, and M. Quack, *J. Comput. Chem.* **16**, 207 (1995).
- ¹⁵R. Signorell, R. Marquardt, M. Quack, and M. A. Suhm, *Mol. Phys.* **89**, 297 (1996).
- ¹⁶R. Marquardt and M. Quack, *J. Chem. Phys.* **109**, 10628 (1998).
- ¹⁷T. J. Lee, J. M. L. Martin, and P. R. Taylor, *J. Chem. Phys.* **102**, 254 (1995).
- ¹⁸H. Hollenstein, R. Marquardt, M. Quack, and M. A. Suhm, *Ber. Bunsenges. Phys. Chem.* **99**, 275 (1995).
- ¹⁹S. Carter, H. M. Shnyder, and J. M. Bowman, *J. Chem. Phys.* **110**, 8417 (1999).
- ²⁰X.-G. Wang and E. L. Sibert III, *J. Chem. Phys.* **111**, 4510 (1999).
- ²¹R. Marquardt, M. Quack, and I. Thanopoulos, *J. Phys. Chem. A* **104**, 6129 (2000).
- ²²S. Carter and J. M. Bowman, *J. Phys. Chem. A* **104**, 2355 (2000).
- ²³D. Papoušek and M. R. Aliev, *Molecular Vibrational-Rotational Spectra* (Elsevier, Amsterdam, 1982).
- ²⁴J.-P. Champion, M. Loëte, and G. Pierre, in *Spectroscopy of the Earth's Atmosphere and Interstellar Medium*, edited by K. N. Rao and A. Weber (Academic, Boston, 1992), p. 339.
- ²⁵M. Quack, *Mol. Phys.* **34**, 477 (1977).
- ²⁶M. Quack, in *Studies in Physical and Theoretical Chemistry*, edited by J. Maruani and J. Serre (Elsevier, Amsterdam, 1983), Vol. 23, p. 355.
- ²⁷D. Uy, M. Cordonnier, and T. Oka, *Phys. Rev. Lett.* **78**, 3844 (1997).
- ²⁸K. S. Pitzer, *Annu. Rev. Phys. Chem.* **38**, 1 (1987).
- ²⁹P. L. Chapovsky and L. J. F. Hermans, *Annu. Rev. Phys. Chem.* **50**, 315 (1999).
- ³⁰D. N. Kozlov, A. M. Prokhorov, and V. V. Smirnov, *J. Mol. Spectrosc.* **77**, 21 (1979).
- ³¹D. L. Gray, A. G. Robiette, and A. S. Pine, *J. Mol. Spectrosc.* **77**, 440 (1979).
- ³²A. G. Robiette, *J. Mol. Spectrosc.* **86**, 143 (1981).
- ³³(a) O. Robert, J.-C. Hilico, M. Loëte, J.-P. Champion, and L. R. Brown, *J. Mol. Spectrosc.* **209**, 14 (2001); (b) See also the internet site of the Dijon group: <http://www.u-bourgogne.fr/LPUB/methane/metspec.htm>
- ³⁴D. Romanini, A. A. Kachanov, and F. Stoeckel, *Chem. Phys. Lett.* **270**, 538 (1997).
- ³⁵B. A. Paldus, C. C. Harb, T. G. Spence, B. Wilke, J. Xie, J. S. Harris, and R. N. Zare, *J. Appl. Phys.* **83**, 3991 (1998).
- ³⁶Y. He, M. Hippler, and M. Quack, *Chem. Phys. Lett.* **289**, 527 (1998).
- ³⁷M. Hippler and M. Quack, *Chem. Phys. Lett.* **314**, 273 (1999).
- ³⁸J. Martin, B. A. Paldus, P. Zalicki, E. H. Wahl, T. G. Owano, J. S. Harris, Jr., C. H. Kruger, and R. N. Zare, *Chem. Phys. Lett.* **258**, 63 (1996).
- ³⁹J. J. Scherer, J. B. Paul, A. O'Keefe, and R. J. Saykally, *Chem. Rev.* **97**, 25 (1997).
- ⁴⁰C. M. Lovejoy and D. J. Nesbitt, *Rev. Sci. Instrum.* **58**, 807 (1987).
- ⁴¹H. Hollenstein, M. Quack, and E. Richard, *Chem. Phys. Lett.* **222**, 176 (1994).
- ⁴²Y. He, H. B. Müller, M. Quack, and M. A. Suhm (to be published).
- ⁴³R. A. Toth, *Appl. Opt.* **33**, 4851 (1994).
- ⁴⁴W. V. Norris and H. J. Unger, *Phys. Rev.* **43**, 467 (1933).
- ⁴⁵A. R. W. McKellar, *Can. J. Phys.* **67**, 1027 (1989).
- ⁴⁶V. M. Blunt, D. L. Cedeno, and C. Manzanares, *Mol. Phys.* **91**, 3 (1997).
- ⁴⁷B. Bobin, *J. Phys. (Paris)* **33**, 345 (1972).
- ⁴⁸K. T. Hecht, *J. Mol. Spectrosc.* **5**, 355 (1960).
- ⁴⁹K. Fox, *J. Mol. Spectrosc.* **9**, 381 (1962).
- ⁵⁰H. A. Jahn, *Proc. R. Soc. London, Ser. A* **168**, 469 (1938).
- ⁵¹J. T. Hougen, *J. Chem. Phys.* **37**, 1433 (1962).
- ⁵²J. T. Hougen, *J. Chem. Phys.* **55**, 1122 (1971).
- ⁵³H. C. Longuet-Higgins, *Mol. Phys.* **6**, 445 (1963).
- ⁵⁴M. Hamermesh, *Group Theory and its Application to Physical Problems* (Addison-Wesley, Reading, MA, 1962).
- ⁵⁵K. Fox and I. Ozier, *J. Chem. Phys.* **52**, 5044 (1970).
- ⁵⁶M. Quack, dissertation EPF Lausanne, these No. 203, 1975, Table 5 (published in *extenso* by EPFL, 1975).
- ⁵⁷G. Herzberg, *Molecular Spectra and Molecular Structure* (Van Nostrand, Toronto, 1945), Vol. II.
- ⁵⁸G. Tarrago, M. Dang-Nhu, G. Poussigue, G. Guelachvili, and C. Amiot, *J. Mol. Spectrosc.* **57**, 246 (1975).
- ⁵⁹I. Ozier, M. C. L. Gerry, and A. G. Robiette, *J. Phys. Chem. Ref. Data* **10**, 1085 (1981).
- ⁶⁰J. Moret-Bailly, *J. Mol. Spectrosc.* **15**, 344 (1965).
- ⁶¹J. Moret-Bailly, L. Gautier, and J. Montagutelli, *J. Mol. Spectrosc.* **15**, 355 (1965).
- ⁶²J. P. Champion, J. C. Hilico, and L. R. Brown, *J. Mol. Spectrosc.* **133**, 244 (1989).
- ⁶³A. De Martino, R. Frey, and F. Pradere, *Chem. Phys. Lett.* **100**, 329 (1983).
- ⁶⁴J. C. Hilico, J. Degni, J. P. Champion, and G. Guelachvili, *J. Mol. Spectrosc.* **81**, 277 (1980).
- ⁶⁵A. De Martino, R. Frey, and F. Pradere, *Chem. Phys. Lett.* **95**, 200 (1983).
- ⁶⁶J. C. Hilico (private communication to L. Halonen, 1996); cited in Ref. 10(c).
- ⁶⁷M. Dang-Nhu, A. S. Pine, and A. G. Robiette, *J. Mol. Spectrosc.* **77**, 57 (1979).
- ⁶⁸A. Mourbat, A. Aboumajd, and M. Loëte, *J. Mol. Spectrosc.* **190**, 198 (1998).
- ⁶⁹K. Fox, *Phys. Rev. A* **8**, 658 (1973).
- ⁷⁰K. Fox and W. B. Person, *J. Chem. Phys.* **64**, 5218 (1976).
- ⁷¹R. Herman and R. F. Wallis, *J. Chem. Phys.* **23**, 637 (1955).
- ⁷²H. M. Hanson and H. H. Nielsen, *J. Mol. Spectrosc.* **4**, 468 (1960).
- ⁷³A. G. Robiette and I. M. Mills, *J. Mol. Spectrosc.* **77**, 48 (1979).
- ⁷⁴R. N. Zare, *Angular Momentum* (Wiley, New York, 1988).